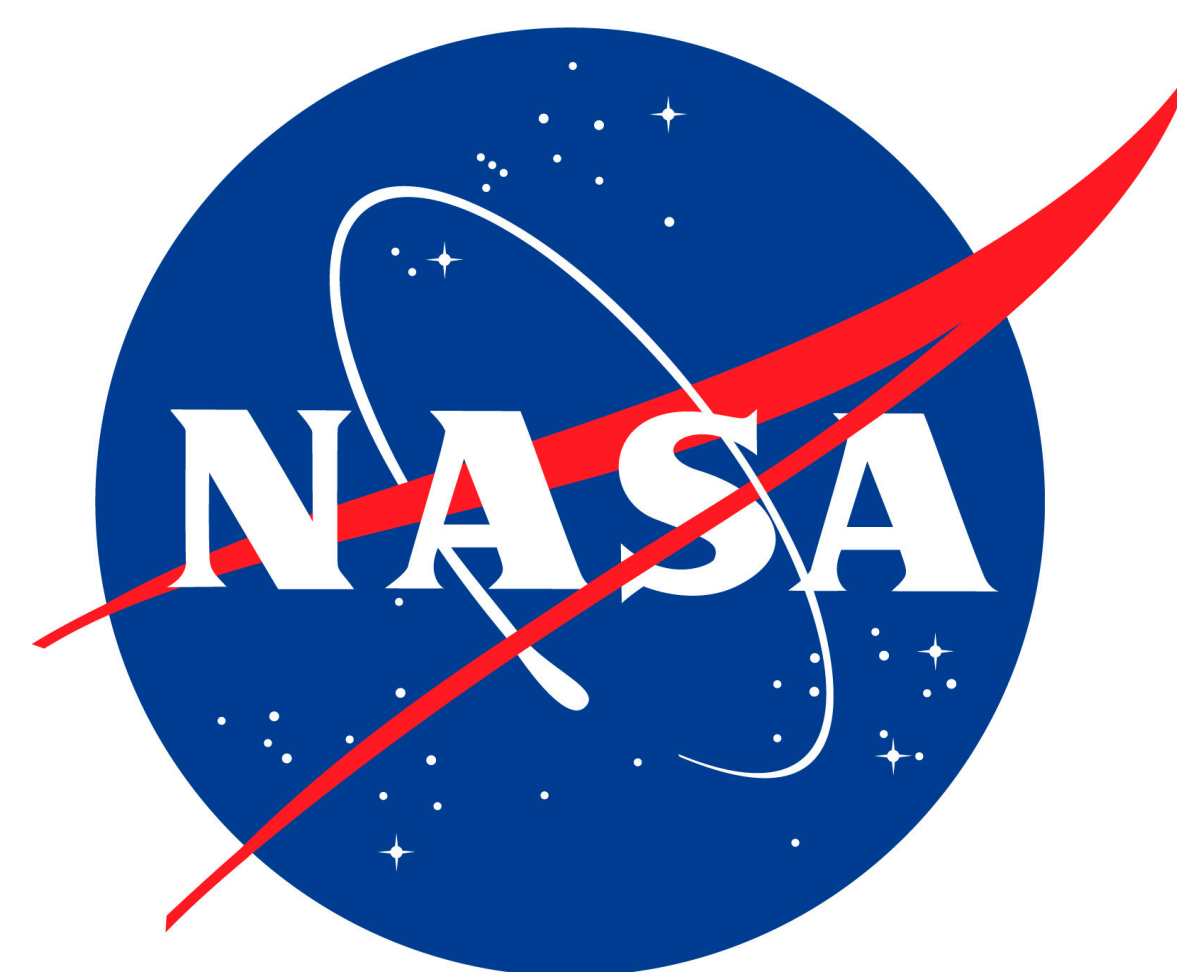


# Identifying Ice Crystal Chain Aggregates in Cold-Season Storms: Leveraging Machine Learning to Map Occurrence and Distribution



Christian M. Nairy<sup>1</sup>, David J. Delene<sup>1</sup>, Shawn W. Wagner<sup>1</sup>, Joseph A. Finlon<sup>2,3</sup>, John E. Yorks<sup>2</sup>

<sup>1</sup>University of North Dakota, Department of Atmospheric Science, Grand Forks, North Dakota, USA

<sup>2</sup>National Aeronautics and Space Administration (NASA), Goddard Space and Flight Center, Greenbelt, Maryland, USA

<sup>3</sup>Earth System Science Interdisciplinary Center (ESSIC), University of Maryland, College Park, Maryland, USA



## Introduction

- Chain Aggregate: Unusually elongated, quasi-linear ice crystal aggregate consisting of  $\geq 3$  discernible ice monomers joined together end-to-end or by small joints.
- Lab studies show chain aggregation is enhanced under strong electric fields ( $> 60 \text{ kV m}^{-1}$ ) at approximately  $-8 \text{ }^\circ\text{C}$  (Saunders & Wahab, 1975).
- In situ observations show chain aggregates (Fig. 1) across diverse cloud regimes and regions, in both summer (a) and winter storms (b).

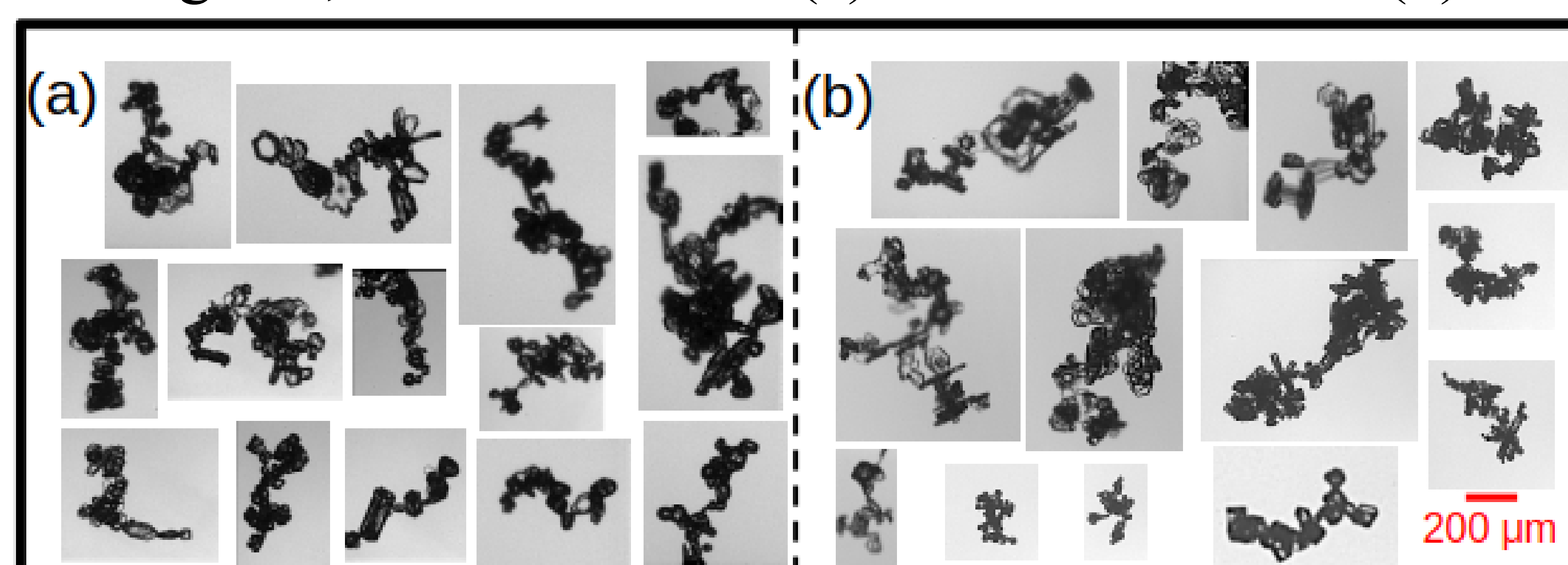


Fig. 1) In situ images of chain aggregates observed during (a) the CapeEx19 Field Campaign and (b) the NASA Investigation of Microphysics and Precipitation for Atlantic Coast-Threatening Snowstorms (IMPACTS) field campaign.

- Strong E-Field lab result  $\neq$  broad winter occurrence in observations  $\rightarrow$  our current picture is incomplete.

## Motivation & Objective

- 1) Chain aggregate formation is not fully understood, and they are not explicitly represented in cloud microphysical parameterizations.
- 2) This gap can affect interpretations of precipitation processes, cloud radiative transfer, and remote-sensing retrievals.
- 3) Manual particle classification is too time-intensive for campaign-scale datasets.

- **Objective:** Train a convolutional neural network (CNN) to automatically detect chain aggregates from Cloud Particle Imager (CPI) imagery and distinguish them from other ice habits (Fig. 2).

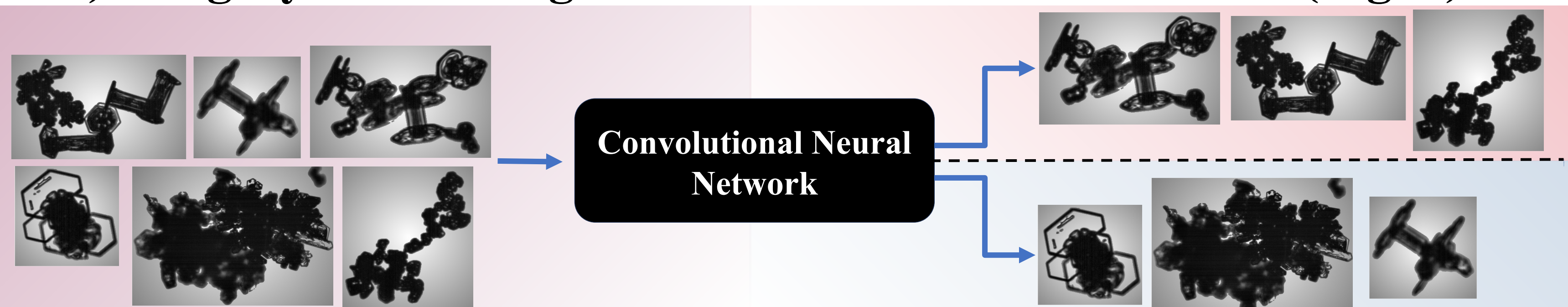


Fig. 2) A simple schematic of what we want the CNN to accomplish. CPI images are ingested into the trained CNN where the chain aggregates are identified and segregated from the total CPI particle population.

## Data & Methods

- Compile CPI imagery from the NASA IMPACTS campaign (Fig. 3).

- Manually classify 56,191 ice particles ( $D_{\text{max}} > 150 \text{ }\mu\text{m}$ ) from multiple flights for training.

- Train/validate/test multiple transfer-learning CNN architectures and select the best-performing model.

- Deploy the optimized CNN across all CPI images ( $\sim 2.3$  million; 33 flights) to map occurrence and distribution.

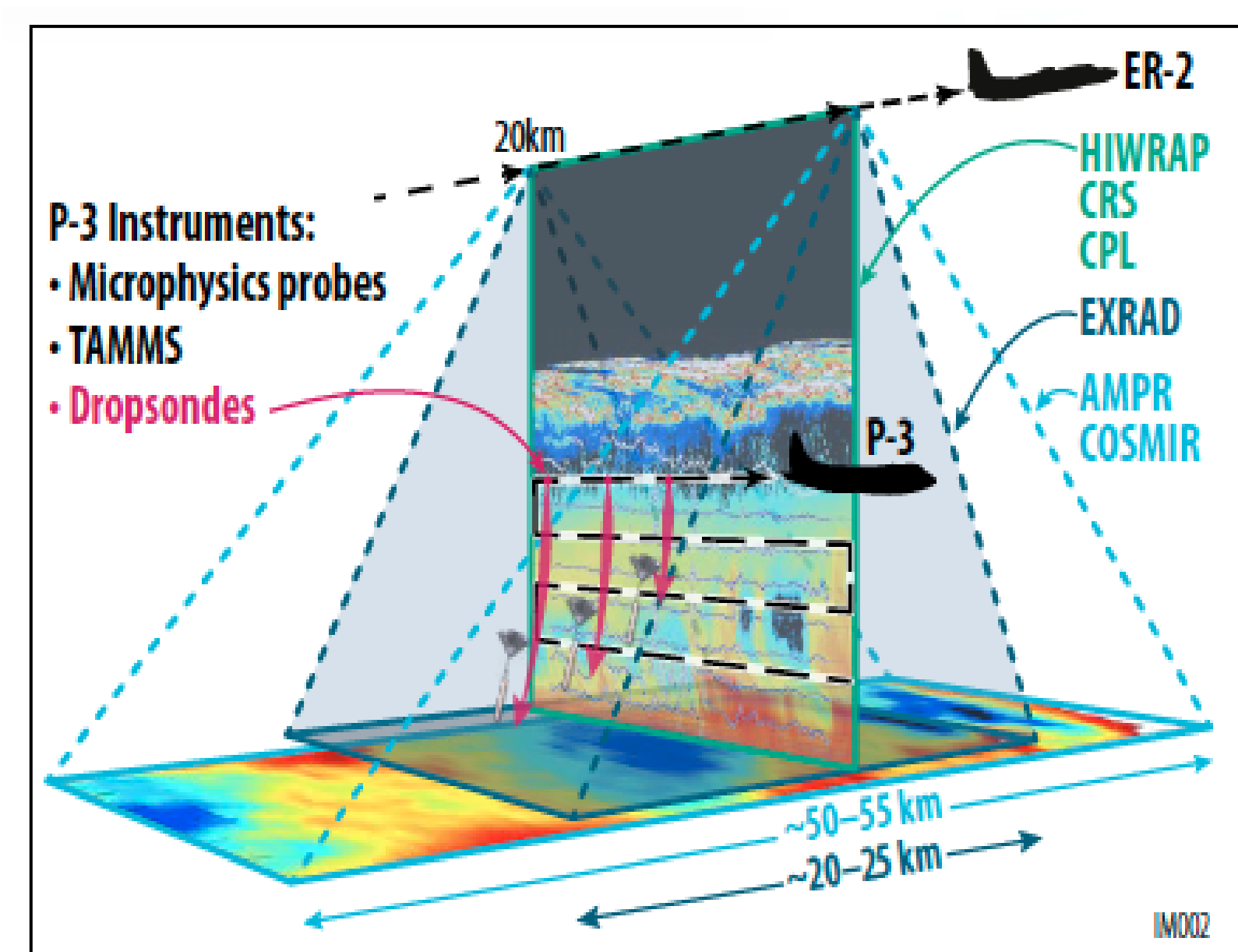
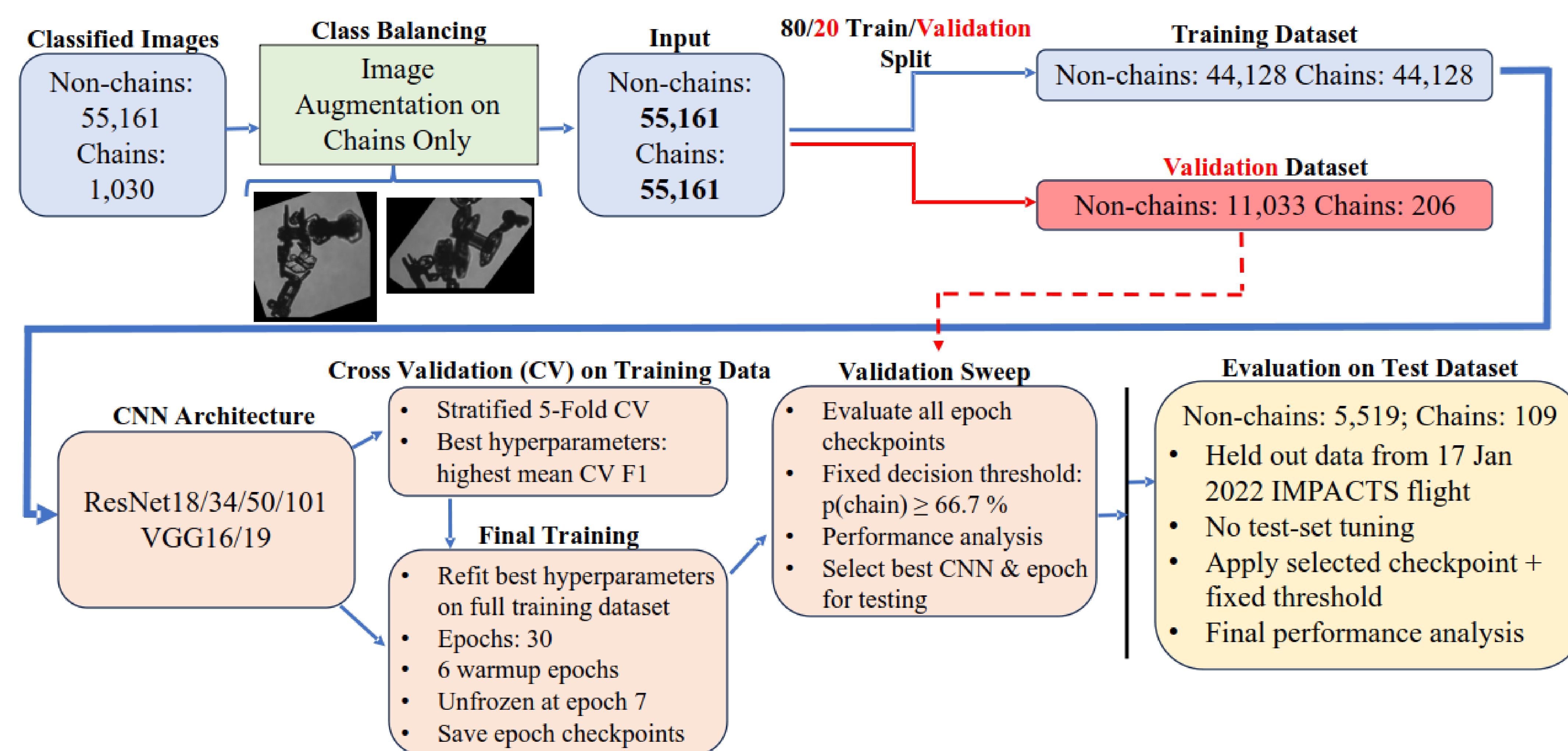


Fig. 3) Typical sampling strategy during the IMPACTS campaign. Adapted from the IMPACTS executive summary (<https://espo.nasa.gov/impacts/>)

## CNN Architecture



## CNN Validation Results

Table 1) Top 5 model/epoch combinations from the validation dataset.

Model	Epoch	Precision	F1	FP	FN	TP	TN	ECE	Brier	Logloss
ResNet34	23	0.9318	0.8586	12	42	164	11021	0.0021	0.0038	0.0133
ResNet50	23	0.918	0.8638	15	38	168	11018	0.0027	0.0037	0.0162
<b>ResNet34</b>	<b>18</b>	<b>0.9135</b>	<b>0.8645</b>	<b>16</b>	<b>37</b>	<b>169</b>	<b>11017</b>	<b>0.0014</b>	<b>0.0038</b>	<b>0.0132</b>
ResNet50	30	0.9135	0.8645	16	37	169	11017	0.003	0.0039	0.0175
ResNet101	26	0.9021	0.875	19	31	175	11014	0.0031	0.0039	0.0181

- Calibration & reliability: ResNet34 has the lowest LogLoss/Brier and tight spread  $\rightarrow$  most reliable across folds.
- ResNet34's stability + calibration makes it the safer default. **Epoch 18** found to maximize precision and maintain balance.

## CNN Testing Results

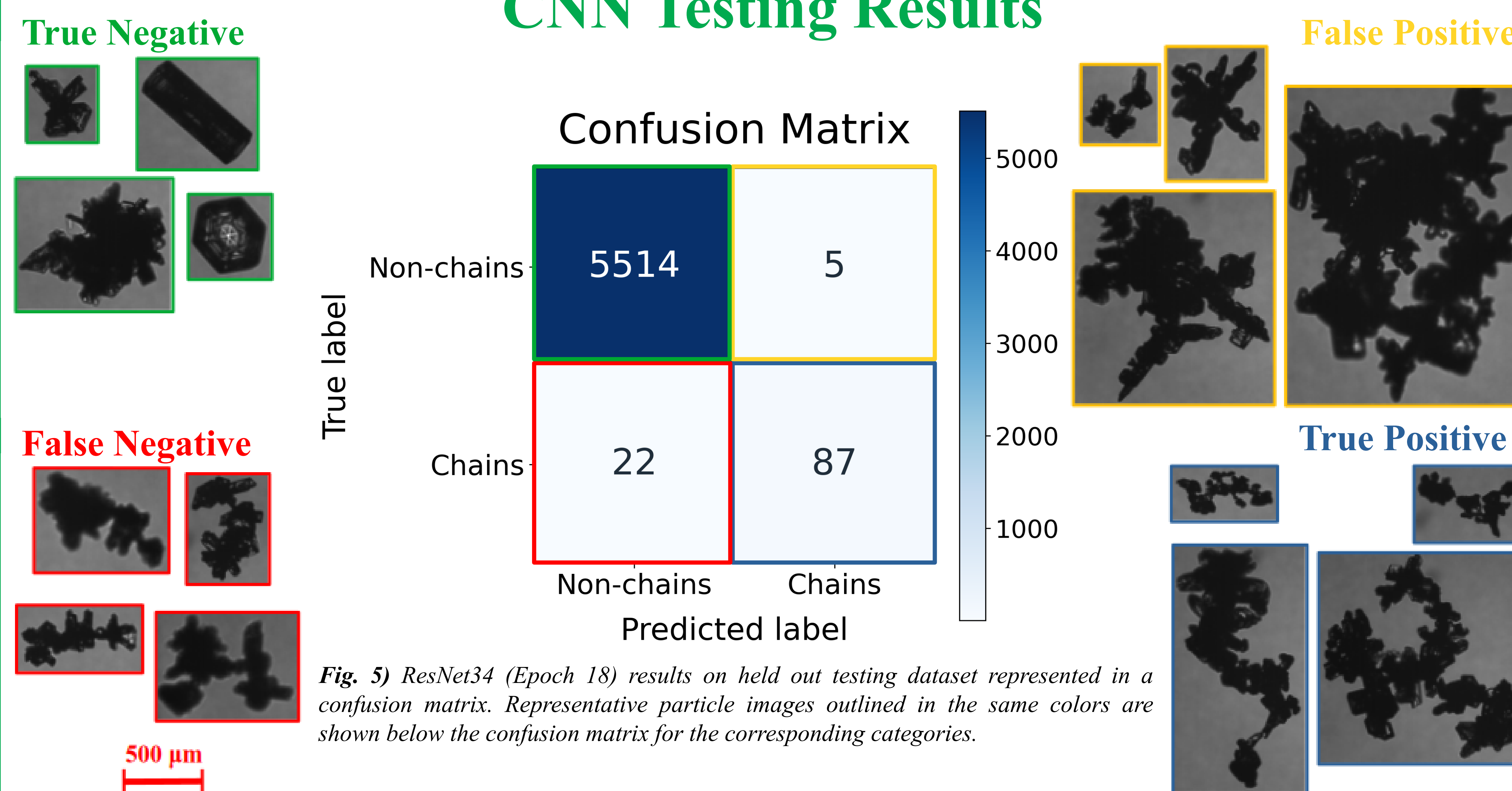


Fig. 5) ResNet34 (Epoch 18) results on held out testing dataset represented in a confusion matrix. Representative particle images outlined in the same colors are shown below the confusion matrix for the corresponding categories.

Table 2) ResNet34 (Epoch 18) results on held out testing dataset.

	Precision	Recall	F1-Score	Support
Non-chains	100%	100%	100%	5519
Chain Aggregates	<b>95%</b>	80%	87%	109
Macro Avg. Accuracy	97%	90%	93%	5628

- ResNet34 delivers few false alarms while retaining strong chain aggregate detections.
- Results from testing the trained ResNet34 model on unseen data verifies that we can be confident in its output on the remaining IMPACTS CPI dataset.

## Using the CNN to Map Occurrence and Distribution

Table 3) Summary of CNN-identified ice crystal chain aggregates by cyclone type during IMPACTS.

Cyclone Type	# of Flights	Sampling Duration (h)	# of CNN Predicted Chains	# of Chains per 20 km
Tropical Cyclone	1	2,009	2316	67.244
Miller B	3	5,934	1453	14.046
Miller A	9	30,267	6805	11.597
Alberta Clipper	2	7,489	667	5.244
Arctic Front	8	23.24	2307	5.123
Great Plains Cyclone	8	25,477	2363	4.697
Jet Streak	1	2,566	60	1.88

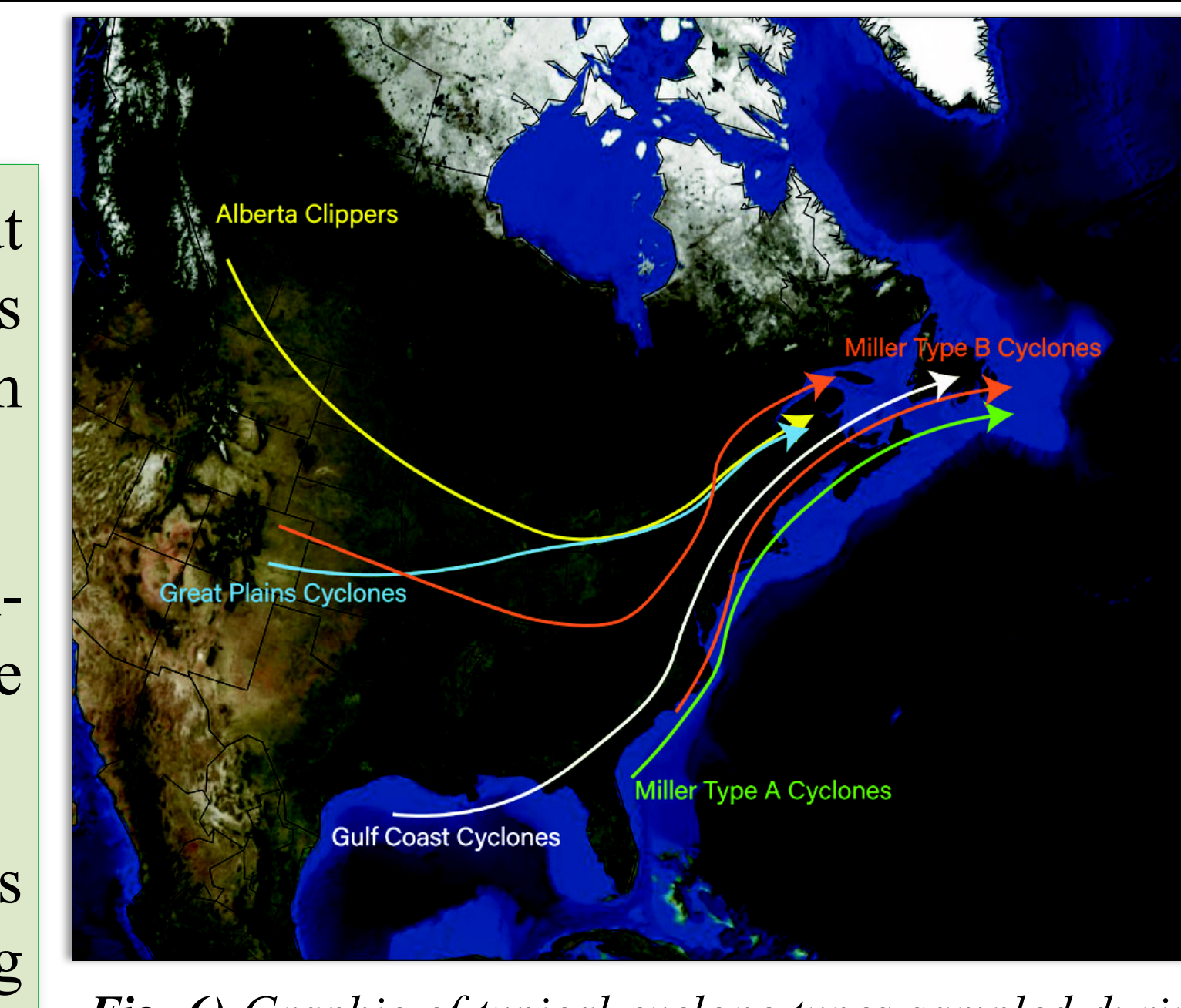


Fig. 6) Graphic of typical cyclone types sampled during IMPACTS. Adapted from Lundstrom et al. 2025 (DOI: <https://doi.org/10.1175/JAS-D-24-0198.1>).

- Tropical Cyclones show the highest chain rate, but this result is based on only one sampled case. This case was also the most electrically active system observed during IMPACTS.
- Miller B Cyclones have the highest chain-aggregate rate among the primary winter cyclone classes ( $\sim 14$  chains / 20 km).
- Miller A Cyclones also exhibit elevated chain rates ( $\sim 12$  chains / 20 km), despite longer sampling duration.

Figure 7) Temperature dependence of CNN-identified ice crystal chain aggregates during IMPACTS science-leg (on-station) periods. Chain occurrence is aggregated within  $2.5^\circ\text{C}$  aircraft ambient temperature bins and normalized by along-track distance (20 km). Error bars denote  $1\sigma$  Poisson counting uncertainty based on the total number of chain detections in each bin, with exposure given by the summed distance across all included flights.

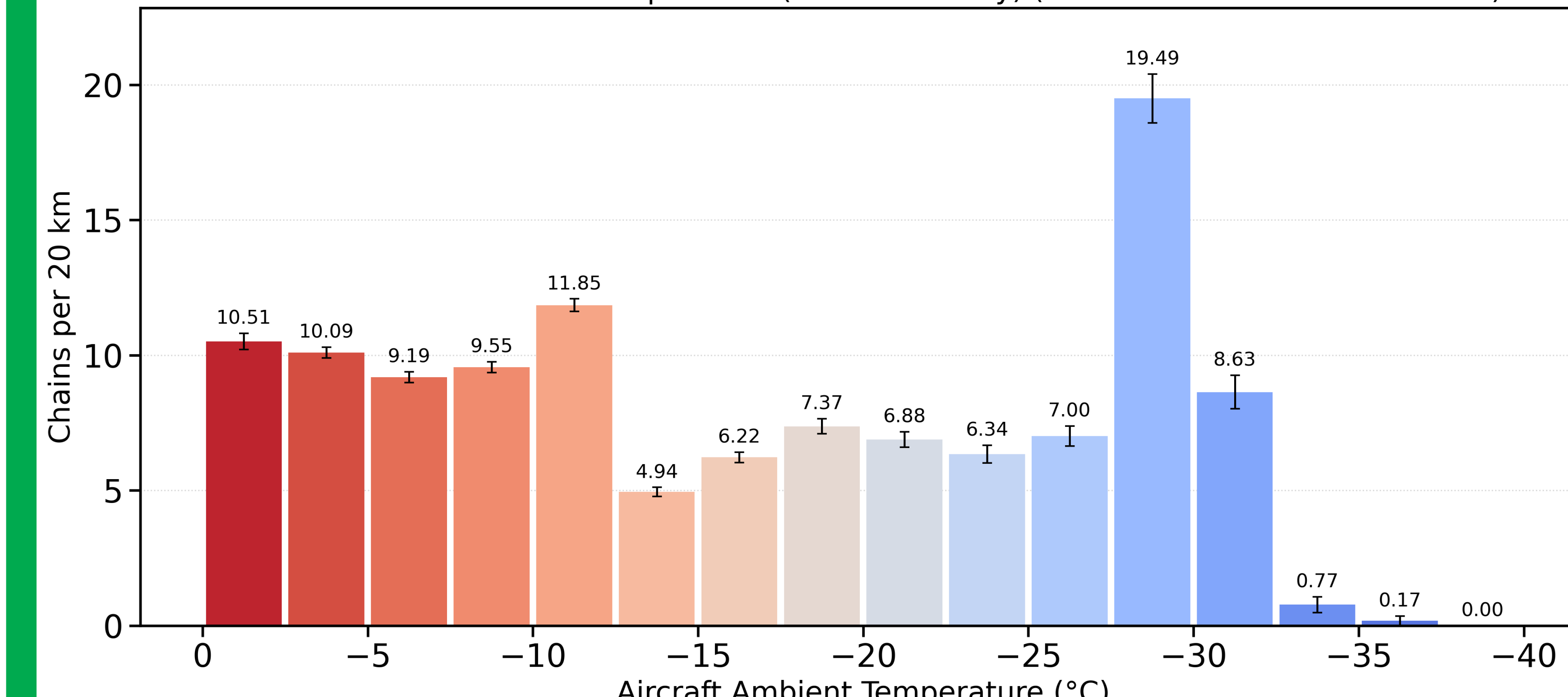


Figure 7) Temperature dependence of CNN-identified ice crystal chain aggregates during IMPACTS science-leg (on-station) periods. Chain occurrence is aggregated within  $2.5^\circ\text{C}$  aircraft ambient temperature bins and normalized by along-track distance (20 km). Error bars denote  $1\sigma$  Poisson counting uncertainty based on the total number of chain detections in each bin, with exposure given by the summed distance across all included flights.

- After distance normalization, chain aggregate occurrence reaches a maximum near  $-30 \text{ }^\circ\text{C}$  ( $\sim 19$  chains per 20 km).
- This distribution may indicate two possible source regions for chain aggregates ( $> -13 \text{ }^\circ\text{C}$  and  $-25$  to  $-33 \text{ }^\circ\text{C}$ )?

## Conclusions & Future Work

- We have developed a CNN that can accurately detect chain aggregates from in situ CPI imagery which can be used to map campaign-scale detections.
- Future work will further interpret the spatio-temporal variability of chain-aggregate occurrence across IMPACTS flights by mapping their distributions within storm life cycles and environmental context.

## References & Acknowledgments

- (1) Nairy, C. M., Delene, D. J., Finlon, J. A., Yorks, J. E., Järvinen, E., Schnaier, M., et al. (2026). In situ observations of ice crystal chain aggregates in winter storms. *Geophysical Research Letters*, 53, <https://doi.org/10.1029/2025GL118365>
- (2) Nairy, C. M. (2022). Observations of chain aggregates in Florida cirrus cloud anvils on 3 August 2019 during CAPEX19. (Master's thesis). Dept. of Atmospheric Sciences, University of North Dakota, Grand Forks, North Dakota.
- (3) Saunders, C. P. R., & Wahab, N. M. A. (1975). The influence of electric fields on the aggregation of ice crystals. *Journal of the Meteorological Society of Japan*, Series II, 53(2), 121–126.

This research is supported by a National Aeronautics and Space Administration (NASA) MOSAICS grant to the University of North Dakota (Grant #: 80NSSC25K7971).

